DELTA-P1 MODEL IMPLEMENTATION FOR NUMERICAL SIMULATION OF PHOTOTHERMAL CANCER THERAPY IN TWO-DIMENSIONAL HETEROGENEOUS TISSUES

ROBERTO C. GOMEZ[1], CARLOS A. BUSTAMANTE[2],RAUL A. VALENCIA[3],WHADY F. FLOREZ[4]

[1] Universidad Pontificia Bolivariana
Circular 1ª 70-01, barrio Laureles, Medellín (Antioquia, Colombia)
roberto.gomeza@upb.edu.co

[2] Universidad Pontificia Bolivariana
Circular 1ª 70-01, barrio Laureles, Medellín (Antioquia, Colombia)
carlos.bustamante@upb.edu.co

[3] Universidad Pontificia Bolivariana
Circular 1ª 70-01, barrio Laureles, Medellín (Antioquia, Colombia)
raul.valencia@upb.edu.co

[4] Universidad Pontificia Bolivariana
Circular 1ª 70-01, barrio Laureles, Medellín (Antioquia, Colombia)
whady.florez@upb.edu.co

Key words: Photothermal therapy (PTT), deep tissues, heterogeneous tissues with nanoparticles, heat transfer models, Delta-P1 model, finite element method

Abstract. Photothermal therapy (PTT) stands as a promising avenue for cancer treatment. Metallic nanoparticles (NPs) absorb near-infrared light, inducing localized heating for tumor cell apoptosis. Predicting spatial temperature information in preclinical models is crucial due to cell death sensitivity to temperature changes. Heat transfer models, rely on the radiative transport equation (RTE), where its approximation is essential for this purpose. Existing models for the radiative transport equation, such as the Beer-Lambert law, the diffusion approximation, the discrete ordinates method, and Monte Carlo (MC) simulations, are widely used in the context of PTT. However, each of them has limitations.

This study focuses on the $\delta P1$ model, wich is an extension of the diffusion approximation. Unlike standard diffusion approximation (SDA), the $\delta P1$ model treats forward and scattered light independently, preserving accuracy over a wider range of optical properties, including media with plasmonic NPs. The $\delta P1$ model equations are discretized and solved by the Finite Element Method (FEM) . Its numerical results for fluence rate in a heterogeneous geometry with nanoshells is compared to MC simulations and the standard diffusion approximation. This study validates and applies the model to the simulation of light transport in photothermal therapy in general two-dimensional geometries. Results demonstrate the $\delta P1$ shows a significant

improvement over the SDA in heat transfer simulations in heterogeneous tissues geometries. This underscores its potential as a valuable tool for optimizing photothermal therapy preclinical models.

1 INTRODUCTION

Cancer is one of the diseases with the highest incidence globally. This clinical condition is the leading cause of death, with a number of 10 million deaths globally in 2020 [1] . Current therapeutic approaches for cancer, primarily encompassing chemotherapy, radiotherapy and surgical intervention, unavoidably exhibit limitations in clinical application [2]. Advancements in oncology have led to the recognition of several alternative cancer therapies, including photodynamic therapy, and photothermal therapy (PTT) [3]. PTT, in particular, stands out for its noninvasive and targeted approach.

Photothermal therapy involves the irradiation of electromagnetic waves to a tissue with a carcinoma, inducing a localized increase in temperature or hyperthermia, which results in cell death mediated by the apoptosis mechanism [4, 2]. Metallic nanoparticles, such as gold nanoparticles, are optimal candidates for this treatment due to their intrinsic property, the resonant surface plasmon. This phenomenon involves the excitation of the nanoparticle at a specific wavelength, resulting in the generation of electric fields around the nanoparticle and an efficient conversion of light into thermal energy through electron and phonon interactions [4].

Numerical modeling of PTT is an invaluable tool for predicting tissue response and temperature distribution in a domain where the therapy is being performed. [5]. PTT modeling is a phenomenon with two components to consider: heat transport and radiative transport [6].It is well known that the Pennes Bioheat model is a useful tool for predicting temperatures in a living tissue. The model integrates biological heat sources, including metabolic activity and blood perfusion [7].

The heat generated by nanoparticles is a source term in bioheat equation in terms of the absorption coefficient and the fluence rate. The fluence rate is obtained by solving the radiative transfer equation (RTE). Previous studies have demonstrated that the selection of the radiative transport model can significantly impact temperature predictions in agar gels. [8, 9]. Notable models used in PTT for approximating the RTE include the Beer-Lambert law, Monte Carlo (MC) simulations, and the standard diffusion approximation (SDA) [10, 11, 12, 9]. SDA has been used extensively to approximate fluence rate and heat generated by nanoparticles in scattering media such as tissues [13, 9]. Nevertheless, the model loses accuracy when scattering coefficient is not relatively larger than absorption coefficient [14, 8, 13]. MC method, which provides a probabilistic estimate of the RTE, is preferred for studying biological tissues due to its superior accuracy compared to deterministic methods like SDA, especially across a broader spectrum of optical properties, refractive index variations and heterogeneous tissue geometries [15]. However, its computational cost prevents its application as a forward model [14]. To overcome the limitations of SDA while maintaining its computational efficiency, other approx-

imations has been explored, such as general spherical harmonics expansion with higher-order terms [16]. Among these models, the $\delta P1$ model stands out, as it retains the order of the harmonic expansion from SDA while providing a more accurate solution across a wider range of optical properties and refractive index mismatches between tissues. The model was firstly proposed to be applied to biological tissues by Prahl [17]. Its ability to maintain accuracy in tissues with high absorption coefficients, such as tissues with embedded nanoparticles, makes it a promising approximation for modeling heat transfer in photothermal therapy.

To the best of the author's knowledge, the implementation of the $\delta P1$ model in two-dimensional heterogeneous geometries has not yet carried out in detail. This article specifically focuses on implementing the model in arbitrary domains as described in the literature, while also comparing its accuracy against SDA and MC methods.

2 MATHEMATICAL MODELLING

2.1 LIGHT TRANSPORT

The transport of visible or infrared photons through a turbid medium, such as tissue, is described by the Radiative Transfer Equation (RTE). Solving this equation involves the use of an approximation of the RTE in conjunction with a set of optical properties of the material, which vary with wavelength. These properties include the absorption coefficient, scattering coefficient, and the angular distribution of scattering, also known as the phase function [18]. Approximating the RTE with spherical harmonics leads to a first-order approximation, the P_1 model, also known as the SDA. The delta Eddington approximation to the phase function yields the δP_1 model. The models' equations are presented in the following sections.

2.1.1 STANDARD DIFFUSION MODEL

In SDA, the fluence rate is described by Eq. 1 [19], where, ϕ is the fluence rate (Wm^{-2}) and μ_a is the absorption coefficient (m^{-1}). The diffusion coefficient D is given by Eq. 2 [19], where the reduced scattering coefficient μ_s^* is given by Eq. 3, where g is the anisotropy factor.

$$-D\nabla^2\phi + \mu_a\phi = S \tag{1}$$

$$D = \frac{1}{3\left(\mu_a + \mu_s^*\right)} \tag{2}$$

$$\mu_s^* = (1 - g)\,\mu_s \tag{3}$$

Laser in the SDA is modelled as a dirichlet boundary condition, given by

$$\phi|_{\partial\Omega_1} = P_0 \tag{4}$$

Where P_0 is the laser irradiance (Wm^{-2}) on the irradiated surface $(\partial\Omega_1)$ In boundaries where the tissue is not being irradiated $(\partial\,\Omega_2)$, an extrapolated boundary is imposed, represented by

$$-D\frac{\partial\phi}{\partial\vec{n}}\bigg|_{\partial\Omega_2} = 2\xi\phi \tag{5}$$

Where ξ represents the boundary mismatch between the air and the domain [9].

2.1.2 $\delta P1$ MODEL

In the $\delta P1$ approximation, the phase function, which describes the angle at which light is bent in a scattering event, is represented with a delta function. It describes collimated and diffuse radiations. This function applied to the RTE allows its reduction to a diffusion equation [17]. Expanding diffusive radiance of the RTE with Legendre polynomials leads to Eq. 6.

$$\nabla^2\phi_d - \mu_{eff}^2\phi_d = -3\mu_s^* \left(\mu_{tr} + \mu_t^*g^*\right)\phi_c \tag{6}$$

Where ϕ_d and ϕ_c represent the diffuse and collimated components of the fluence rate $(\mathrm{W\,m^{-2}})$. The effective attenuation coefficient is defined as $\mu_{\mathrm{eff}} = \sqrt{3\mu_a\mu_{\mathrm{tr}}}$. The isotropic scattering coefficient is given by $\mu_s' = \mu_a + \mu_s\left(1 - g\right)$, while the reduced scattering coefficient is denoted by μ_s^*, defined in Eq. 3. The transport coefficient is $\mu_{\mathrm{tr}} = \mu_a + \mu_s'$, and $\mu_t^* = \mu_a + \mu_s^*$, all with units of $(\mathrm{m^{-1}})$.

According to Prahl, ϕ_c can be obtained by numericlally solving [17]

$$\frac{\partial\phi_c}{\partial\hat{s_0}} = -\mu_t^*\left(\vec{x}\right)\phi_c \tag{7}$$

Where $\hat{s_0}$ represents the direction of the collimated radiation.

Recalling that the phase function splitted radiation into collimated and diffuse component, it is proposed that the first two moments of the phase function are function of the fraction of light scattered forward. Where the first moment g is defined as the square of the fraction, and the second is given by [16]

$$g^* = \frac{g}{1+g} \tag{8}$$

When diffuse light is incident on a slab with different refraction index, it is required conservation of the diffuse flux component normal to the surface, which is given by [16].

$$\left(\phi_d - Ah\frac{\partial\phi_d}{\partial\vec{n}}\right)\bigg|_{\partial\Omega} = -3Ahg^*\mu_s^*\phi_c \tag{9}$$

Where h is given by Eq. 10, and A is a coefficient that describes radiation reflected due to Fresnel reflection [16]. Calculating this coefficient, leads to the approximation of the Fresnel reflection moments R_1 and R_2. By evaluating through numerical integration on a normal slab, the coefficient has been fitted to a cubic polynomial, given by Eq. 11 [17].

$$h = \frac{2}{3\mu_{tr}} \tag{10}$$

$$A = -0.13755n^3 + 43390n^2 - 4.09466n + 168960 \tag{11}$$

Where n is the ratio between air and tissue refraction index.

By solving equations 7 and 6 subject to Eq. 9, ϕ_c and ϕ_d are summed to compute the total fluence rate, which is then inserted to the bioheat equation as a source term.

2.2 HEAT TRANSPORT MODEL

The linear bioheat equation is given by [7]

$$\rho C_p \frac{\partial T}{\partial t} = k\nabla^2 T + Q_m + Q_b + \mu_a \phi \tag{12}$$

Where C_P is the specific heat of the tissue, Q_m is heat generated by metabolic processes, Q_b is the blood perfusion term and $\mu_a \phi$ is heat generated by nanoparticles, where ϕ is the fluence rate calculated in light transport model.

When a tissue is exposed to ambient temperature, a heat flux is generated due to the temperature differences at the interface. This flux is represented as a Robin boundary condition, given by [20]

$$-k\frac{\partial T}{\partial \vec{n}}\bigg|_{\partial\Omega} = h\left(T - T_{ref}\right) \tag{13}$$

3 MATERIALS AND METHODS

3.1 GEOMETRY AND MESH

Lopes et al. proposed an experimental geometric setup to test the implementation of MC and SDA model [9]. This setup involves a cube enclosing an inner cylinder containing GNPs. As the localized heating and temperature measurements are away from the boundaries, in which no effect from boundaries should be observed, a modified geometry is proposed, including an outer cylinder with the embedded GNP region, shown in Fig. 1a. Taking advantage of the axis symmetry of the proposed geometry, a axisymmetric mesh was generated using GMSH [21], taking a wedge of the original case . Regions and elements are highlighted in Fig. 1.

3.2 MONTE CARLO SIMULATIONS

Monte Carlo method was implemented using MCX from Monte Carlo Studio [22]. The Geometry was loaded using basic shapes in volume designer with the dimensions of validation case. A voxel size of $0.125\ mm$ was used for the simulations with 10^8 photons for the validation case. For the light source, a gaussian beam was configured with a waist radius of $7\ mm$ [9]. Fluence rate was integrated and scaled in a time span of $1\ s$ to get the steady state behavior for the fluence. Results were interpolated to degrees of freedom (DOF) in the heat transport model mesh using linear interpolation.
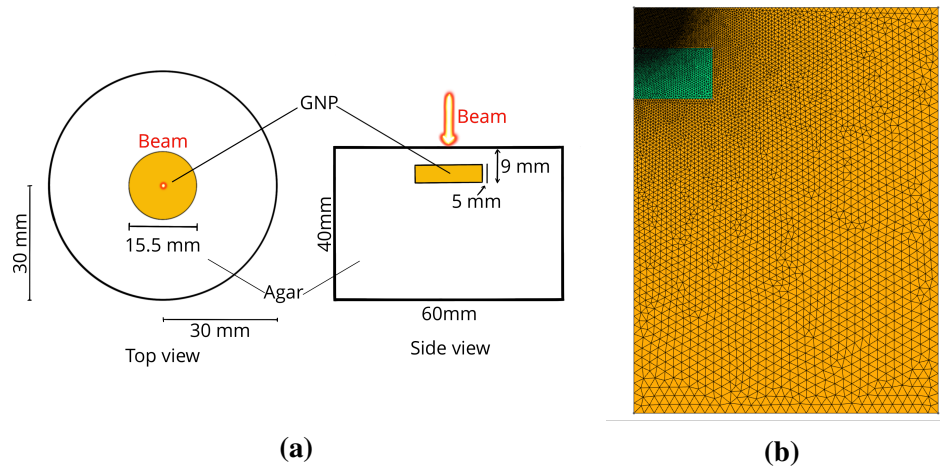
Figure 1: Mesh and geometry. (a) Modified case geometry from Lopes et. al [9]. (b) 2D mesh.

3.3 SDA SIMULATIONS

Equation 1 was expressed in cylindrical coordinates, discretized and solved by the Finite Element Method (FEM) using the open source framework FEniCSx, composed by DOLFINX, basix and UFL [23, 24, 25]. A variational form from the equation was formulated using Galerkin method with a Lagrange first order function space for the mesh shown in Fig 1. Laser BC was modelled using Eq. 4, with an equivalent beam radius of 11 mm [9]. The resulting linear system was solved using Portable, Extensible Toolkit for Scientific Computation (PETSc) LU decomposition direct solver [26].

3.4 $\delta P1$ MODEL

Equation 7 was solved for every DOF of a DOLFINx function defined in the mesh using 4th order Runge Kutta method provided by Scipy Solve_ivp function [27]. Taking and initial value of fluence rate at the corresponding surface point of each DOF. Fluence rate at surface was taken as a gaussian distribution of full width half maximum (FWHM) corresponding to the MC simulation. The resulting function was taken as the source term in the solution of the Eq. 6, with the same method as SDA for discretizing the domain and solving the linear system.

3.5 HEAT TRANSPORT SIMULATION

For obtaining transient behavior of temperature given by Eq. 12, the model was expressed in cylindrical coordinates and discretized spatially using FEniCSx [23, 24, 25]. A backward implicit euler algorithm was implemented for time stepping, with a dt of 0.1 s. The corresponding linear system for each time step was solved using PETSc BigSTAB iterative solver [26].

6

Table 1: Optical properties measured in subdomains from Lopes et. al [9].

Property	Gel	GNP
$\mu_a \ (m^{-1})$	2	31
$\mu_s \ (m^{-1})$	176	289

3.6 VALIDATION CASE

Experimental case proposed by Lopes et. al is modelled using the modified geometry shown in Fig. 1a [9]. The authors made an agar gel phantom with embedded gold nanoparticles in a cylindrical shaped subdomain. The gel was irradiated with a gaussian beam with FWHM and power of 7 mm and 1.1 W respectively [9]. The top surface of the domain was modelled with a robin boundary condition given by Ec. 13, taking a convection coefficient of 5 $W K^{-1} m^{-2}$. The other boundaries were taken as zero flux condition [9]. Optical properties of the domains were determined by the authors, shown in table 1. Other properties such as index refraction, specific heat, density and thermal conductivity were considered equal to water properties reported in literature [28]. The gel phantom was irradiated 706 s.

4 RESULTS AND DISCUSSION

4.1 VALIDATION

(a)

(b)

(c)
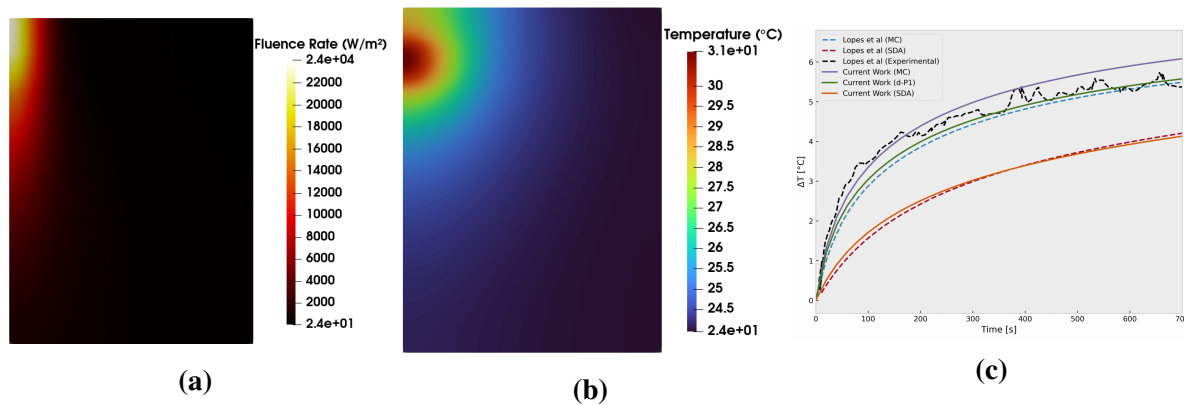
Figure 2: Fluence rate (a), temperature field (b) in MC validation case and temperature over time (b) measured in $r = 0mm$, $z = 4mm$ simulated and reported by Lopes et. al [9]

Lopes et. al experimental configuration is particularly useful for numerically implementing photothermal therapy (PPT), as tumor irradiation often targets deep tissues. This approach ensures that therapy is applied while minimizing its invasive effect [29].

To confirm that the current model is being applied correctly, the results of Lopes et al. were used as reference values for validation purposes. [9]. Results and experimental data obtained

from the authors are shown in Fig. 2. Fluence rate generated by the gaussian beam calculated from MC method is shown in Fig. 2a, showing the absorption and scattering effects of the phantom. A temperature field at 706 s is obtained in Fig. 2b. At $r = 0$, 4 mm below the surface, the authors measured the temperature during irradiation time [9]. As shown in Fig. 2c, the agreement between the experimental results and the proposed models indicates the reliability of the $\delta P1$ model since temperatures are close o reported measurements and MC results. However, several differences in the MC curve may be attributed to voxel resolution and uncertainty regarding the MC boundary conditions.

4.2 MODELS COMPARISON

(a)

(b)

(c)
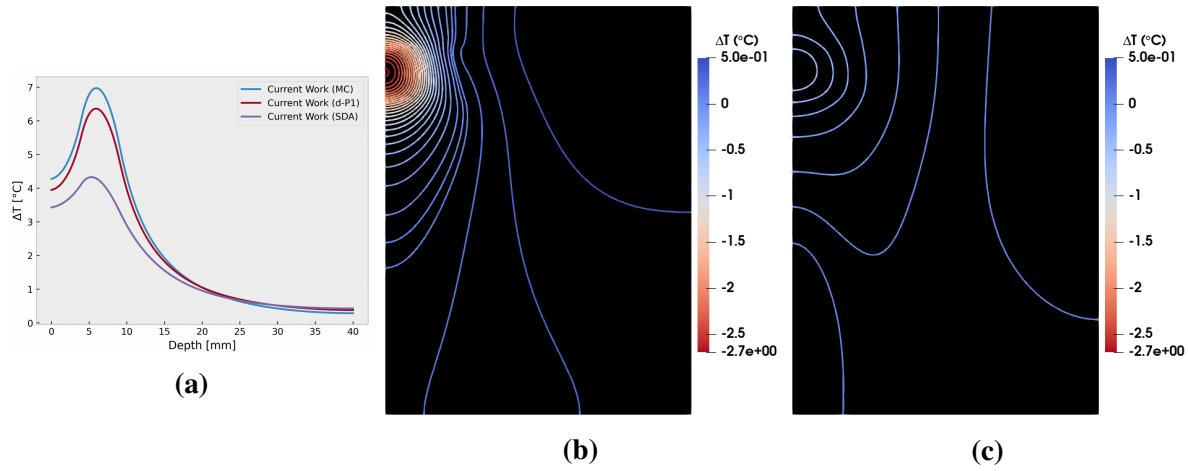
Figure 3: Models comparison at t = 706 s simulation time. (a) Temperature over the laser axis. (b) SDA local error. (c) $\delta P1$ local error.

$\delta P1$ model was applied to the validation case to compare its approximation in contrast to SDA and MC. Figure 3 presents a comparison based on two criteria. Fig 3a shows the temperature over the cylinder axis. A temperature maximum value is evident at the depth where the GNPs are located, indicating the presence of absorption heterogeneity. This result is consistent with the reported by Lopes et. al [9]. When the $\delta P1$ is compared to SDA, a notable increase in the maximum temperature is observed, representing an enhancement of the SDA in approximately 80%.

In PPT, it is crucial to consider not only the maximum temperature in the tumor but also the temperature in the surrounding tissue [30]. Figures 3c and 3b shows local error at 706 s with respect to the temperature filed shown in Fig. 2b. As previosuly reported by several authors, SDA greatly underestimate temperatures in the GNP region [13]. On the other hand, $\delta P1$ model performs well both within and outside the GNP region. The highest temperature difference observed was 0.6 °C, which outperformed the SDA. This is explained as the $\delta P1$ threads forward and scatters light independently, allowing for greater generalization on forward

8

scattering media such as tissues. This, in turn, results in a wider range of optical properties, where the model maintains its accuracy. [31].

5   CONCLUSIONS

$\delta P1$ model is assessed as comprehensive radiative transport model to be applied to study laser-induced thermal effects in a gel phantom mimicking a deep tissue configuration with embedded gold nanoparticles (GNPs) subjected to PTT. The simulation workflow encompassed geometric modeling, mesh generation, and solving radiative and heat transport equations. The $\delta P1$ model demonstrated remarkable agreement with Monte Carlo (MC) simulations in predicting laser-induced thermal behavior within the gel phantom containing gold nanoparticles (GNPs). This agreement underscores the efficacy and accuracy of the $\delta P1$ model in capturing the essential physics of photon absorption and subsequent heat generation within the tissue. The successful alignment between the $\delta P1$ model and MC simulations highlights its potential as a practical tool for researchers in the field of biomedical optics. This validation paves the way for broader utilization of the model in photothermal therapy, where precise heat deposition predictions are crucial for optimizing treatment outcomes.

REFERENCES

[1] W. H. O. Who, "Cáncer," *World Health Organization: WHO*, Feb. 2022.

[2] S. Liao, W. Yue, S. Cai, Q. Tang, W. Lu, L. Huang, T. Qi, and J. Liao, "Improvement of Gold Nanorods in Photothermal Therapy: Recent Progress and Perspective," *Front. Pharmacol.*, vol. 12, p. 664123, Apr. 2021.

[3] H. S. Han and K. Y. Choi, "Advances in Nanomaterial-Mediated Photothermal Cancer Therapies: Toward Clinical Applications," *Biomedicines*, vol. 9, Mar. 2021.

[4] X. Huang, I. H. El-Sayed, W. Qian, and M. A. El-Sayed, "Cancer Cell Imaging and Photothermal Therapy in the Near-Infrared Region by Using Gold Nanorods," *J. Am. Chem. Soc.*, vol. 128, pp. 2115–2120, Feb. 2006.

[5] M. Asadi, J. Beik, R. Hashemian, S. Laurent, A. Farashahi, M. Mobini, H. Ghaznavi, and A. Shakeri-Zadeh, "MRI-based numerical modeling strategy for simulation and treatment planning of nanoparticle-assisted photothermal therapy," *Phys. Med.*, vol. 66:124-132., Oct. 2019.

[6] Y. Ren, Y. Yan, and H. Qi, "Photothermal conversion and transfer in photothermal therapy: From macroscale to nanoscale," *Adv. Colloid Interface Sci.*, vol. 308, p. 102753, Oct. 2022.

[7] M. A. Giordano, G. Gutierrez, and C. Rinaldi, "Fundamental solutions to the bioheat equation and their application to magnetic fluid hyperthermia," *Int. J. Hyperthermia*, Aug. 2010.

[8] A. M. Elliott, J. Schwartz, J. Wang, A. M. Shetty, C. Bourgoyne, D. P. O'Neal, J. D. Hazle, and R. J. Stafford, "Quantitative comparison of delta P1 versus optical diffusion approximations for modeling near-infrared gold nanoshell heating," *Med. Phys.*, vol. 36, pp. 1351–1358, Apr. 2009.

[9] A. Lopes, R. Gomes, M. Castiñeras, J. M. P. Coelho, J. P. Santos, and P. Vieira, "Probing deep tissues with laser-induced thermotherapy using near-infrared light," *Lasers Med. Sci.*, vol. 35, pp. 43–49, Feb. 2020.

[10] S. Soni, H. Tyagi, R. A. Taylor, and A. Kumar, "Investigation on nanoparticle distribution for thermal ablation of a tumour subjected to nanoparticle assisted thermal therapy," *J. Therm. Biol.*, vol. 43, pp. 70–80, July 2014.

[11] J. C. G. Jeynes, F. Wordingham, L. J. Moran, A. Curnow, and T. J. Harries, "Monte Carlo Simulations of Heat Deposition during Photothermal Skin Cancer Therapy Using Nanoparticles," *Biomolecules*, vol. 9, Aug. 2019.

[12] I. V. A. K. Reddy, S. Elmaadawy, E. P. Furlani, and J. M. Jornet, "Photothermal effects of terahertz-band and optical electromagnetic radiation on human tissues," *Sci. Rep.*, vol. 13, pp. 1–11, Sept. 2023.

[13] A. M. Elliott, R. J. Stafford, J. Schwartz, J. Wang, A. M. Shetty, C. Bourgoyne, P. O'Neal, and J. D. Hazle, "Laser-induced thermal response and characterization of nanoparticles for cancer treatment using magnetic resonance thermal imaging," *Med. Phys.*, vol. 34, pp. 3102–3108, July 2007.

[14] H. Xu, T. J. Farrell, and M. S. Patterson, "Investigation of light propagation models to determine the optical properties of tissue from interstitial frequency domain fluence measurements," *J. Biomed. Opt.*, vol. 11, p. 041104., July 2006.

[15] C. Zhu and Q. Liu, "Review of Monte Carlo modeling of light transport in tissues," in *Journal of Biomedical Optics, Vol. 18, Issue 5*, vol. 18, p. 050902, SPIE, May 2013.

[16] S. A. Carp, S. A. Prahl, and V. Venugopalan, "Radiative transport in the delta-P1 approximation: Accuracy of fluence rate and optical penetration depth predictions in turbid semi-infinite media," *J. Biomed. Opt.*, vol. 9, pp. 632–47, May 2004.

[17] S. A. Prahl, *Light Transport in Tissue*. PhD thesis, University of Texas at Austin, 1988.

[18] A. E. Profio, "Light transport in tissue," *Appl. Opt.*, vol. 28, pp. 2216–2222, June 1989.

[19] R. Zhang, W. Verkruysse, G. Aguilar, and J. S. Nelson, "Comparison of diffusion approximation and Monte Carlo based finite element models for simulating thermal responses to laser irradiation in discrete vessels," *Phys. Med. Biol.*, vol. 50, pp. 4075–86, Oct. 2005.

[20] T.-C. Shih, P. Yuan, W.-L. Lin, and H.-S. Kou, "Analytical analysis of the Pennes bioheat transfer equation with sinusoidal heat flux condition on skin surface," *Med. Eng. Phys.*, vol. 29, pp. 946–953, Nov. 2007.

[21] C. Geuzaine and J.-F. Remacle, "Gmsh: A 3-D finite element mesh generator with built-in pre- and post-processing facilities," *Int. J. Numer. Methods Eng.*, vol. 79, pp. 1309–1331, Sept. 2009.

[22] "Monte Carlo eXtreme - Physically accurate and validated photon ray-tracer," May 2024. [Online; accessed 13. May 2024].

[23] "DOLFINx: The next generation FEniCS problem solving environment," May 2024. [Online; accessed 13. May 2024].

[24] M. W. Scroggs, I. A. Baratta, C. N. Richardson, and G. N. Wells, "Basix: a runtime finite element basis evaluation library," *Journal of Open Source Software*, vol. 7, p. 3982, May 2022.

[25] M. S. Alnæs, A. Logg, K. B. Ølgaard, M. E. Rognes, and G. N. Wells, "Unified form language: A domain-specific language for weak formulations of partial differential equations," *ACM Trans. Math. Software*, vol. 40, pp. 1–37, Mar. 2014.

[26] S. Balay, S. Abhyankar, M. F. Adams, S. Benson, J. Brown, P. Brune, K. Buschelman, E. M. Constantinescu, L. Dalcin, A. Dener, V. Eijkhout, J. Faibussowitsch, W. D. Gropp, V. Hapla, T. Isaac, P. Jolivet, D. Karpeev, D. Kaushik, M. G. Knepley, F. Kong, S. Kruger, D. A. May, L. C. McInnes, R. T. Mills, L. Mitchell, T. Munson, J. E. Roman, K. Rupp, P. Sanan, J. Sarich, B. F. Smith, S. Zampini, H. Zhang, H. Zhang, and J. Zhang, "PETSc Web page." https://petsc.org/, 2024.

[27] "scipy.integrate.solve_ivp — SciPy v1.13.0 Manual," Apr. 2024. [Online; accessed 13. May 2024].

[28] E. Engineeringtoolbox, "Water - Thermophysical Properties," Oct. 2023. [Online; accessed 15. May 2024].

[29] X. Wu, Y. Suo, H. Shi, R. Liu, F. Wu, T. Wang, L. Ma, H. Liu, and Z. Cheng, "Deep-Tissue Photothermal Therapy Using Laser Illumination at NIR-IIa Window," *Nano-Micro Letters*, vol. 12, Dec. 2020.

[30] Y.-T. Ren, H. Qi, Q. Chen, and L.-M. Ruan, "Thermal dosage investigation for optimal temperature distribution in gold nanoparticle enhanced photothermal therapy," *Int. J. Heat Mass Transfer*, vol. 106, Oct. 2016.

[31] B. Yuan, "Radiative transport in the delta-p1 approximation for laminar optical tomography," *J. Innov. Opt. Health Sci.*, vol. 02, pp. 149–163, Apr. 2009.